

Evaluation of HP β CD–PEG Microparticles for Salmon Calcitonin Administration via Pulmonary Delivery

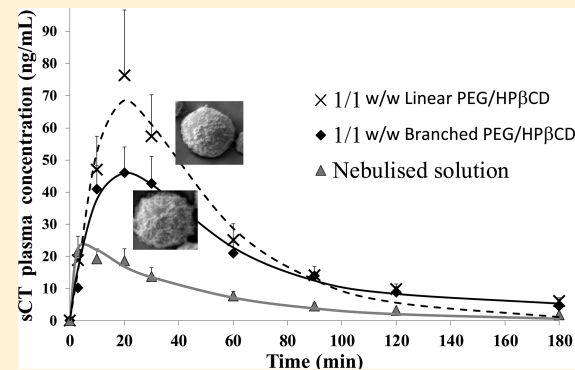
Frederic Tewes,^{†,‡} Oliviero L. Gobbo,[†] Maria I. Amaro,[†] Lidia Tajber,[†] Owen I. Corrigan,[†] Carsten Ehrhardt,[†] and Anne Marie Healy^{*,†}

[†]School of Pharmacy and Pharmaceutical Sciences, University of Dublin, Trinity College Dublin, Dublin 2, Ireland

[‡]INSERM ERI-23, Pôle Biologie-Santé, Faculté de Médecine & Pharmacie, Université de Poitiers, 40 av. du Recteur Pineau, 86022 Poitiers Cedex, France

ABSTRACT: For therapeutic peptides, the lung represents an attractive, noninvasive route into the bloodstream. To achieve optimal bioavailability and control their fast rate of absorption, peptides can be protected by coprocessing with polymers such as polyethylene glycol (PEG). Here, we formulated and characterized salmon calcitonin (sCT)-loaded microparticles using linear or branched PEG (L-PEG or B-PEG) and hydroxypropyl-beta-cyclodextrin (HP β CD) for pulmonary administration. Mixtures of sCT, L-PEG or B-PEG and HP β CD were co-spray dried. Based on the particle properties, the best PEG:HP β CD ratio was 1:1 w:w for both PEGs. In the sCT-loaded particles, the L-PEG was more crystalline than B-PEG. Thus, L-PEG-based particles had lower surface free energy and better aerodynamic behavior than B-PEG-based particles. However, B-PEG-based particles provided better protection against chemical degradation of sCT. A decrease in sCT permeability, measured across Calu-3 bronchial epithelial monolayers, occurred when the PEG and HP β CD concentrations were both 1.6 wt %. This was attributed to an increase in buffer viscosity, caused by the two excipients. sCT pharmacokinetic profiles in Wistar rats were evaluated using a 2-compartment model after iv injection or lung insufflation. The maximal sCT plasma concentration was reached within 3 min following nebulization of sCT solution. L-PEG and B-PEG-based microparticles were able to increase T_{max} to 20 ± 1 min and 18 ± 8 min, respectively. Furthermore, sCT absolute bioavailability after L-PEG-based microparticle aerosolization at 100 μ g/kg was 2.3 times greater than for the nebulized sCT solution.

KEYWORDS: dry powder inhalation, peptide, pulmonary delivery, pharmacokinetic, Calu-3, permeability, crystallinity, surface free energy, cyclodextrin, PEG



1. INTRODUCTION

Salmon calcitonin (sCT) has been approved for the treatment of bone diseases. Because peptides such as sCT have a poor bioavailability when taken orally, they are typically administered via parenteral injection, and sCT is currently marketed as an injectable solution (Miacalcin). However parenteral administration is painful and often leads to low patient compliance. Hence, new noninvasive delivery strategies for sCT have been explored, such as pulmonary administration¹ or nasal sprays; the latter are currently marketed (Fortical, Miacalcin). Nonetheless, the nasal formulations show a very wide bioavailability, ranging from 0.3% to 30.6%, compared to the same dose by intramuscular injection.^{2,3} Here, we investigated the new possibility of pulmonary delivery of sCT as a powder.

The vast epithelium of the lungs is a promising route for sCT delivery. In contrast to the gastrointestinal tract, lungs provide much higher absorption of peptides, with much less metabolism.⁴ Hence, for sCT, the lung is an attractive, noninvasive route into the bloodstream. Nevertheless, to achieve optimal bioavailability (protection from peptidases and clearance mechanisms) and prolong its

therapeutic action, sCT could be coadministered with stabilizing excipients such as polyethylene glycol (PEG) and hydroxypropyl-beta-cyclodextrin (HP β CD). In fact, the covalent binding of PEG to peptides to increase their half-life *in vivo*⁵ and reduce their immunogenicity⁶ is a common approach. Currently, a number of pegylated peptides are marketed. Some studies have evaluated the biological potentials of pegylated sCT derivatives after pulmonary administration.⁷ However, no reported studies have investigated whether it is of importance to covalently bind PEG to the peptide in the case of pulmonary administration. Most formulation production processes are stressful for peptides, leading to a potential loss of their activity. PEG can protect the peptides from activity loss during the formulation process.⁸ Also, PEG polymer helps to engineer the particle surface to reduce particle–particle and *in vivo* particle–protein interactions and reduce particle clearance by phagocytosis.⁹

Received: May 3, 2011

Accepted: September 1, 2011

Revised: August 28, 2011

Published: September 01, 2011

However, because of their low melting temperature ($T_m \sim 60^\circ\text{C}$), it is difficult to spray dry PEGs with the most frequently used safe solvents, as the outlet temperature in the spray dryer is too close to the PEGs' T_m , leading to fused, aggregated material.^{8,10} To overcome this problem, another excipient with a high T_m or high glass transition temperature (T_g) can be added to the formulation, changing the thermal properties of the system. HP β CD is an amorphous material with a high T_g of around 200 °C, and thus could protect the surface of PEG-based particles from aggregation. More importantly, in solution, HP β CD acts as "chemical chaperone" and inhibits sCT aggregation, thereby increasing its physical stability.^{6,11} Furthermore, some cyclodextrins are known to act as permeability enhancers either by increasing the drug apparent solubility, as for the cyclopeptide FK224,¹² protecting against peptidase action¹¹ or temporarily altering the membrane.¹³ For instance, dimethyl- β -cyclodextrin was able to enhance sCT pulmonary absorption in rats after dry powder administration.¹³ The use of HP β CD or methyl- β -cyclodextrin in pharmaceutical formulations is well established. However, among the cyclodextrins, HP β CD showed the lowest cell toxicity on pulmonary epithelial cell lines.^{14,15} Furthermore, randomly methylated β -cyclodextrin produced an irreversible loss of cell layer barrier function, while perturbations of epithelial integrity were moderate and reversible in the case of HP β CD.¹⁴ As HP β CD is the only modified β CD cited in the FDA's list of Inactive Pharmaceutical Ingredients,¹⁶ its use to develop DPI formulations is preferable to that of methylated β -cyclodextrin.

In the present paper, we describe a process of formulating sCT-loaded microparticles made of PEG and HP β CD and designed for pulmonary delivery. sCT was co-spray dried with linear or branched PEG along with HP β CD to formulate microparticles. Micromeritic, thermodynamic and aerodynamic properties of the prepared microparticles are presented. sCT-loaded particles were also evaluated in terms of loading, sCT physical stability and biological activity. sCT apparent permeability was tested *in vitro* through the Calu-3 epithelial monolayer model. Pharmacokinetic studies in rat were performed for the most promising formulations.

2. MATERIALS AND METHODS

2.1. Materials. Hydroxypropyl- β -cyclodextrin with an average degree of substitution of 0.65 (Encapsin HPB) was purchased from Janssen Biotech, Olen, Belgium. Linear PEG 10 kDa (L-PEG) and alkanes with 99.8% purity (hexane, heptane, octane, nonane, decane and undecane) were purchased from Sigma-Aldrich, Ireland. Four armed branched PEG 10 kDa (B-PEG) were purchased from JenChem Technology Inc., USA. PEGs of 10 kDa were used to ensure their diffusion from the lung into the blood circulation and subsequent renal clearance. Salmon calcitonin acetate salt was obtained from Polypeptide Laboratories, Sweden.

2.2. Methods. **2.2.1. Spray Drying.** sCT, (L-PEG or B-PEG) and HP β CD were spray dried as a solution having a total concentration of 1% w/w using a Büchi B-290 mini spray dryer (Büchi, Flawil, Switzerland) set in the closed cycle mode with a 2-fluid nozzle. Solutions were composed of butyl acetate/methanol/water mixture with a volume ratio 5:5:1. PEG:HP β CD weight ratios were 1:1, 1:3 and 0:1. The spray dryer was operated as follows: Inlet temperature was 65 °C; feeding pump was set at 30%; spraying N₂ nozzle flow rate was 15 L/min; N₂ flowing at 630 L/min was used as the drying gas. These conditions resulted in an outlet temperature ranging from 36 to 39 °C.

2.2.2. Characterization of Physicochemical Properties of the Particles. Scanning Electron Microscopy (SEM). SEM micrographs of samples were taken using a Tescan Mira XMU (Tescan s.r.o., Czech Republic) electron microscope. The samples were fixed on an aluminum stub and coated with a 10 nm thick gold film. Primary electrons were accelerated under a voltage of 5 kV. Images were formed from the collection of secondary electrons.

Butyl Acetate Assay by Gas Chromatography (GC). A GC PerkinElmer Clarus 500 with auto sampler and a Supelco SPB-GC column (60 m × 0.25 mm × 0.5 μm, 35% phenyl 65% dimethyl polysiloxane filling) was used to detect the residual content of butyl acetate in the particles, following the method outlined in the European Pharmacopoeia (2010). Linear calibration curves ($r^2 > 0.999$) were obtained using standard solutions in water with concentrations of butyl acetate ranging from 0.1 to 2.5 mg/mL and 2 mg/mL of ethyl acetate as an internal standard. Samples were prepared by dissolving 200 mg of powder in 1 mL of water. Then, 1 μL of aqueous solution was injected and elution of the organic molecules was monitored over 20 min using a flame ionization detector ($n = 3$). Helium flowing at 1.58 cm³/min was used as a carrier gas. The oven temperature was 50 °C, and the detector temperature was set to 325 °C.

Thermogravimetric Analysis (TGA). TGA was performed using a Mettler TG 50 (Mettler Toledo Ltd, Greifensee, Switzerland). Accurately weighed samples (~10 mg) were analyzed using open aluminum pans under N₂ purge. Samples were run at a heating rate of 10 °C/min from 25 to 200 °C.⁸

Differential Scanning Calorimetric Analysis (DSC). DSC was performed using crimped aluminum pans loaded with 3–5 mg of samples. Samples were heated at a rate of 300 °C/min under helium purge from 10 to 200 °C using a Diamond DSC controlled by the Pyris software (PerkinElmer, Ireland). The % of crystallinity of PEG polymers in the HP β CD–PEG mixtures was calculated as previously described.⁸

Powder X-ray Diffraction (XRD). XRD measurements were conducted on samples placed in a low background silicon holder, using a Rigaku Miniflex II desktop X-ray diffractometer (Rigaku, Tokyo, Japan). The samples were scanned over a range of 5–40° 2θ at a step size of 0.05°/s as previously described.⁸

Particle Size Distribution Analysis. The geometric particle size distributions (PSD) were determined by laser diffraction using a Malvern Mastersizer 2000 (Malvern Instruments Ltd. Worcestershire, U.K.) with the Scirocco 2000 dry powder feeder to disperse the particles as described previously.⁸ The dispersive air pressure used was 3 bar, and vibration feed rate was set to 50%. Data were analyzed based on the equivalent volume median diameter, D_{50} , and the span of the PSD. The PSD of each sample was determined in triplicate.

Dynamic Vapor Sorption (DVS). DVS experiments were performed on a DVS-1 (SMS Ltd., London, U.K.). The DVS-1 measures the vapor mass change with a resolution of ±0.1 μg. The temperature was 25.0 ± 0.1 °C. The samples were exposed to the following % of relative humidity (RH) profile: 0, 3, 5, 10%, then to 90% in 10% steps and the reverse for desorption. At each stage, the sample mass was allowed to reach equilibrium defined as $dm/dt \leq 0.002$ mg/min over 10 min, before the RH was changed. The amount of water uptake for each RH stage was expressed as a % of the dry sample mass (m_0).

Surface Area Measurement. The specific surface area of the samples ($n = 3$) was determined by the N₂ adsorption BET multipoint method, with 6 points in the relative pressure range of 0.1–0.3, using a Micromeritics Gemini 2835c (Micromeritics,

Norcross, USA). Samples were prepared by purging under N₂ overnight at 30 °C.

Surface Free Energy Measurement. Measurements were performed at 0% RH or 40% RH and 30 °C ($n = 3$), using an inverse gas chromatography (iGC) instrument (SMS Ltd, London, U.K.). Powders were packed into a silanized glass columns (300 mm × 3 mm) and then pretreated for 1 h at 30 °C and 0% RH. Then, 250 μL of the probe vapor–helium mixture was injected into the helium flow. All injections of probe vapors were performed at 0.03% v/v of the saturated probe vapor. A flame ionization detector was used to monitor the probe's elution. In acid–base theory, the total surface free energy of a solid (γ_s^T) has 2 main components: a dispersive contribution (γ_s^d) and specific or acid–base contribution (γ_s^{AB}), which are independent and additive. In order to calculate γ_s^d of the particles, alkane probes with a known dispersive contribution (γ_p^d) and a nil specific contribution (γ_p^{AB}) were used. Methane was used as an inert reference. At this low % of saturation (0.03% v/v), iGC was used in infinite dilution conditions and γ_s^d was calculated using the method developed by Schultz et al.¹⁷ γ_s^{AB} was obtained indirectly via the measurement of the specific free energy of adsorption of 2 monopolar probes (ethyl acetate and dichloromethane) and by using the acid–base theories developed by Van Oss et al. (vOCG).¹⁸ In the vOCG theories, γ_s^{AB} is subdivided into two nonadditive parameters γ_s^+ and γ_s^- representing the electron acceptor (acid) and donor (base) properties, respectively. By using ethyl acetate ($\gamma_p^- = 475.67$, $\gamma_p^+ = 0$ mJ/m², at 30 °C) as base probe and dichloromethane ($\gamma_p^- = 0$, $\gamma_p^+ = 124.58$ mJ/m², at 30 °C) as acid probe with the acid–base values calculated based on the Della Volpe and Siboni scale,¹⁹ γ_s^+ and γ_s^- of the particle were calculated.

Aerodynamic Particle Diameter Analysis. The aerodynamic diameter (AD) distribution of the particles was measured using a Next Generation Impactor (NGI) as previously described.⁸ The flow rate was adjusted to get a pressure drop of 4 kPa in the powder inhaler (Handihaler, Boeringher Ingelheim), and the time of aspiration was adjusted to obtain 4 L. The inhaler was filled with a gelatin No. 3 capsule loaded with 20 ± 2 mg of powder ($n = 3$). After inhaler actuation, particle deposition on the NGI was determined by HPβCD assay as described below. The amount of particles with AD ≤ 5.0 μm, expressed as a percentage of the emitted recovered dose, was considered as the fine particle fraction (FPF). The mass median aerodynamic diameter (MMAD) and FPF were calculated as previously described.⁸

HPβCD Assay. HPβCD assay was based on the method described by Higuti et al.²⁰ The concentration of HPβCD was determined by measuring the decrease in absorbance at 550 nm of a phenolphthalein solution due to HPβCD–phenolphthalein complexation. HPβCD standard solutions with concentrations ranging from 0.003 to 0.1 w/v % were prepared in 0.1 M Na₂CO₃/NaHCO₃ buffer, pH 10.3, with a constant phenolphthalein concentration of 0.001 w/v %.

2.2.3. Fourier Transform Infrared Spectroscopy (FTIR) of sCT. Attenuated total reflectance (ATR)-FTIR measurements were performed on the powders. The powders were placed on a wedged diamond crystal, pressed with a force of 80 N, and spectra were then recorded using a Spectrum 400 FT spectrometer (PerkinElmer, Ireland). For each spectrum, 32-scan interferograms were collected with 4 cm⁻¹ resolution. A freshly cleaned crystal surface was used as a reference. The spectra of the excipients and water vapor were subtracted from the sCT spectra

separately, and then sCT spectra were normalized from 1490 to 1780 cm⁻¹.

2.2.4. sCT Loading. sCT HPLC assay was performed using an LC Module I PLUS (Waters, U.K.) chromatographic system with a C18, 15–20 μm, 3.9 × 300 mm column (μ Bondapak, Waters, Ireland) as described previously.⁸ Measurements were conducted by injecting 50 μL of sample, standard (concentration ranged from 0.1 to 0.003 g/L) or control solutions in the mobile phase running at 1.5 mL/min and composed of 64 vol % of aqueous phase (1.8 g/L NaCl, 0.05% v/v TFA in H₂O) and 36 vol % of acetonitrile. sCT was detected by measuring the absorbance at 214 nm. The sCT loading was defined as the mass of sCT divided by the total mass of particles. The loading efficiency was defined as the ratio between the theoretical and practical loading.

2.2.5. sCT Transepithelial Transport across Calu-3 Cell Monolayers. Calu-3 cells were cultured in modified EMEM medium and used between passages 38 and 55. Cell monolayers were obtained by seeding cells (5 × 10⁵ cells/cm²) onto Transwell polyester membrane (Corning, Netherlands), maintained at 37 °C in 5% of CO₂. Medium was replaced every 2 days. Cells were used when the transepithelial electrical resistance was higher than 1000 Ω·cm². Transport experiments were carried out in HEPES buffered Krebs–Ringer (KRB) solution. Monolayers were first equilibrated with buffer for 1 h. The apical solution was then replaced with 0.5 mL of the test solutions containing fluorescein (10 μg/mL). After 60 min at 37 °C, samples were collected from the compartments for sCT and fluorescein assay. sCT was assayed using an ELISA kit (S1155, Bachem, U.K.). Fluorescein was assayed by measuring the fluorescence intensity at 520 nm after excitation at 492 nm using a plate reader (FLUOstar OPTIMA, BMG Labtech, Aylesbury, U.K.). Standard solutions were made in KRB (concentrations ranged from 0.015 to 1 μg/mL). The apparent permeabilities (P_{app} , cm/s) for sCT and fluorescein in the apical-to-basal direction (A→B) were calculated using eq 1:

$$P_{app} = \frac{(C_b V_b)}{(St C_a)} \quad (1)$$

where C_b (mg/mL) was the concentration of sCT or fluorescein and V_b the volume (1.5 mL) of buffer in the basal side, t the incubation time (3600 s) and S the insert surface area (1.12 cm²). C_a (mg/mL) was the initial compound concentration in the apical side ($n = 3$).

2.2.6. Dynamic Viscosity Measurements. Dynamic viscosity (μ , mPa·s) of polymer solutions and polymer:HPβCD (1:1 weight ratio) mix solutions (concentration range was from 1.25 to 20 wt %) was measured at 37 °C using a SV-10 Vibro-viscometer (Malvern Ltd, Worcestershire, U.K.).

2.2.7. Pharmacokinetics. Male Wistar rats (BioResources, TCD, Ireland) weighing 350 ± 50 g were used. The compliance of this study with EC Directive 86/609 was reviewed and approved by the Trinity College Dublin ethical committee. Rats were anesthetized by an intraperitoneal (ip) injection of a mixture of ketamine (Vetalar; Pfizer, Ireland) and medetomidine hydrochloride (Domitor, Pfizer, Ireland) at the doses of 60 mg/kg and 0.5 mg/kg body weight, respectively. Then, in the case of intravenous (iv) administration of sCT, two heparinized permanent polyurethane intravascular tubings were implanted on the day of the experiment. The left femoral vein was cannulated for sCT solution administration, while the left femoral artery was

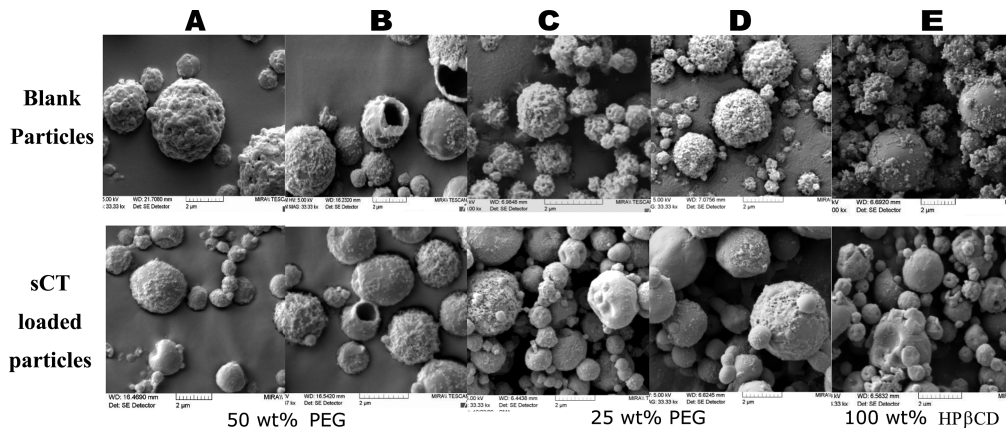


Figure 1. SEM micrographs of particles formulated by spray drying solutions made of various ratios of HP β CD and PEG (linear or branched). Loaded particles were composed of 5 wt % sCT: (A) (1:1) L-PEG:HP β CD, (B) (1:1) B-PEG:HP β CD, (C) (1:3) L-PEG:HP β CD, (D) (1:3) B-PEG:HP β CD, (E) HP β CD.

cannulated for blood sampling. For pulmonary sCT administration, only one catheter was implanted in the left femoral artery for blood sampling.

The iv bolus administration of sCT (100 μ g/kg) was performed by injecting sCT solutions at 70 μ g/mL in 0.9% w/v NaCl. Then, the anesthetic reversal agent, atipamezole hydrochloride solution (Antisedan, Pfizer, Ireland), was injected ip at 5 mg/kg. The sCT dose for pulmonary administration was 100 μ g/kg, which corresponded approximately to the insufflation of 1 mg of dry powder or to the nebulization of 100 μ L of sCT solutions at 350 μ g/mL in 0.9% w/v NaCl. Powder administration was performed using a Dry Powder Insufflator Model DP-4. (Penn-Century, Philadelphia, PA, USA). sCT solution nebulization was performed using an AeroProbe intracorporeal nebulizing catheter controlled by a LabNeb unit (Trudell Medical International, London, U.K.). Anesthetized rats were maintained by the upper incisors on a rodent work stand inclined at 45°. Vocal cords were visualized with the help of an otoscope, and then a plastic guide was inserted between them. The rat was put back to the horizontal position, then the sprayer was introduced into the plastic tube and the formulation was nebulized when the rat was breathing in. The tip was withdrawn and anesthetic reversal agent was injected ip.

Blood samples (200 μ L) were collected in heparinized tubes at the following times: 0; 3; 10; 20; 30; 60; 90; 120; 180 min after sCT administration. In each case, blood was replaced by an equal volume of isotonic solution. Blood samples were centrifuged at 10000 rcf for 5 min. Plasma was withdrawn and kept frozen at -20 °C until sCT assay by ELISA kit (S1155, Bachem, U.K.).

Pharmacokinetic parameters were determined for each individual rat using a two-compartment model. sCT plasma concentration (C_p) versus time profiles were fitted with eq 2 using the least-squares method (Excel, Microsoft, USA).

$$C_p = A e^{-\alpha t} + B e^{-\beta t} + C e^{-K_a t} \quad (2)$$

with $\alpha > \beta$, and $C = 0$ for profile fitting after iv administration, and $C = -(A + B)$ for profile fitting after pulmonary administration. The distribution and elimination phases of C_p versus time profiles were characterized by the half-life times $t_{1/2-\alpha} = \ln 2/\alpha$ and $t_{1/2-\beta} = \ln 2/\beta$, respectively. Area under C_p versus time profiles (AUC) were calculated using the linear trapezoidal rule. The area remaining after the last measured concentration ($C_{t \rightarrow 180}$) was

extrapolated using eq 3.

$$AUC_{t \rightarrow \infty} = \frac{C_{t \rightarrow 180}}{\beta} \quad (3)$$

Bioavailability (F) was calculated by comparison of the sCT AUC extrapolated to infinity obtained after pulmonary administration to that obtained after iv administration at the same dose.

$$F = \frac{AUC_{t \rightarrow \infty}^{\text{pulm}}}{AUC_{t \rightarrow \infty}^{\text{iv}}} \quad (4)$$

The total body clearance of sCT (CL) was calculated as the ratio between the dose of sCT (dose $\times F$) and the corresponding AUC.

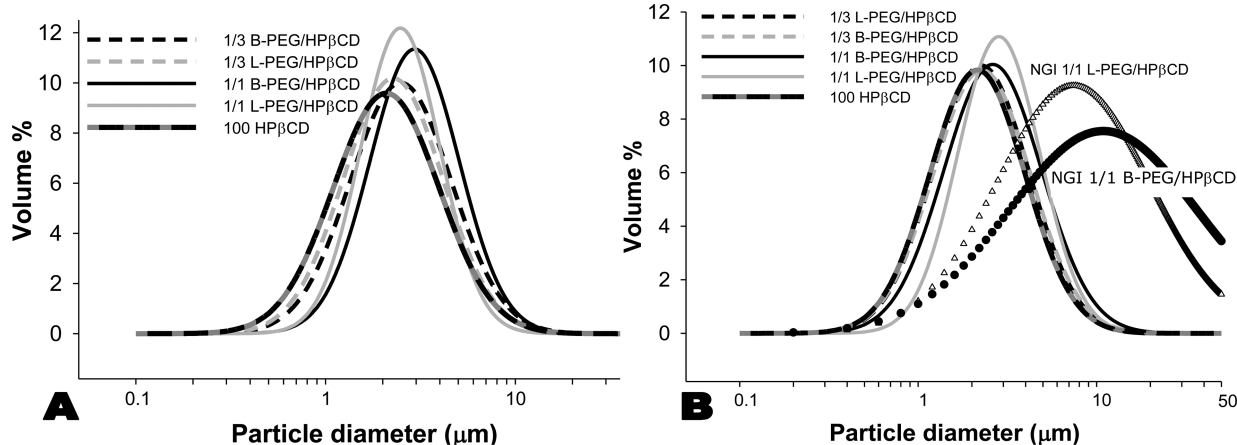
2.2.8. Statistical Data Analysis. Data were statistically evaluated by a Student *t*-test, or a one-way analysis of variance (ANOVA) test with Tukey's multiple comparison test as post hoc test. Significance level was $\alpha < 0.05$.

3. RESULTS

SEM micrographs of spray dried PEG:HP β CD particles are shown in Figure 1. Particles made of L-PEG:HP β CD or B-PEG:HP β CD at a 1:1 weight ratio had different morphologies. Those containing L-PEG were spherical with rough surfaces. Micro-particles made of B-PEG were spherical with nanoparticles attached on their surfaces. However, the two types of particles seemed to be hollow, as observed from the "broken" particles. Loading of sCT into the 1:1 B-PEG:HP β CD particles did not change their morphology in comparison to the blank ones (Figure 1B), whereas the 1:1 L-PEG:HP β CD sCT-loaded particles acquired nanoparticles on their surfaces, similar to the 1:1 B-PEG:HP β CD sCT-loaded particles. A decrease in the PEG:HP β CD ratio to (1:3) led to the formation of microparticles surrounded by nanoparticles for both types of PEG. In comparison to the 1:1 B-PEG:HP β CD particles, the number and the diameter of nanoparticles increased. For these particles, the addition of 5 wt % sCT reduced the number and size of nanoparticles. Particles made of 100% HP β CD were spherical and polydisperse in size, with microparticles and separated nanoparticles. The incorporation of 5 wt % sCT in this formulation seemed to prevent the formation of nanoparticles. sCT loading in the different types of particles ranged from 4.4 ± 0.1 to 5.2 ± 0.2 wt % (Table 1). These values allowed the insufflation of the

Table 1. Physicochemical Characteristics of (A) Blank and (B) sCT-Loaded Particles

(A) Blank Particles											
PEG:HP β CD ratio	type of PEG	D_{50} (μm)	span	PEG $\Delta H_{\text{melting}}$ (J/g)	PEG deg of crystallinity (%)	PXRD ^a	BET surface area (m^2/g)				
(1:1)	L-PEG	2.48 \pm 0.01	1.32	63.3 \pm 4.4	55.4 \pm 3.9	C	4.66 \pm 0.04				
	B-PEG	2.95 \pm 0.01	1.39	57.8 \pm 4.2	65.3 \pm 4.7	C	2.69 \pm 0.24				
(1:3)	L-PEG	2.27 \pm 0.02	1.58	1.1 \pm 0.2	1.9 \pm 0.4	A	8.28 \pm 0.03				
	B-PEG	2.49 \pm 0.01	1.62	6.7 \pm 1.5	15.1 \pm 3.4	A	6.65 \pm 0.03				
(0:1)	no	2.09 \pm 0.01	1.68	NA ^b	NA	A	10.34 \pm 0.01				
(B) sCT Loaded											
PEG:HP β CD Ratio	type of PEG	D_{50} (μm)	span	PEG $\Delta H_{\text{melting}}$ (J/g)	PEG deg of crystallinity (%)	PXRD	$\Delta H_{\text{endotherm}}$ with $T_{\text{onset}} = 122^\circ\text{C}$ (J/g)	% wt loss (TGA)	butyl acetate (ppm)	mean loading wt %	loading efficiency %
(1:1)	L-PEG	2.84 \pm 0.01	1.50	75.7 \pm 3.1	66.3 \pm 2.7	C	4.3 \pm 1.7	2.39	1286 \pm 761	4.4 \pm 0.1	93.3 \pm 2.1
	B-PEG	2.62 \pm 0.01	1.63	43.0 \pm 1.6	48.6 \pm 1.8	C	6.2 \pm 3.1	3.08	<490	5.2 \pm 0.2	111 \pm 3.9
(1:3)	L-PEG	2.27 \pm 0.01	1.62	1.8 \pm 0.4	3.2 \pm 0.7	A	19.4 \pm 3.1	8.18	28727 \pm 1575	4.6 \pm 0.1	96.3 \pm 3.0
	B-PEG	2.26 \pm 0.02	1.60	1.4 \pm 1.6	3.2 \pm 3.6	A	33 \pm 2.1	7.44	22831 \pm 995	5.2 \pm 0.2	107.0 \pm 4.3
(0:1)	no	2.15 \pm 0.01	1.62	NA	NA	A	72.2 \pm 4.0	11.40	37978 \pm 1301	5.2 \pm 0.1	102.6 \pm 2.2

^a A: amorphous. C: crystalline. ^b NA: Not applicable.**Figure 2.** Geometric particle size distribution (PSD) by volume of blank (A) and sCT-loaded particles (B). Aerodynamic size distribution of sCT-loaded (1:1) L-PEG:HP β CD and (1:1) B-PEG:HP β CD particles are shown in (B).

sCT dose (100 $\mu\text{g}/\text{kg}$) into the rat lungs in one administration. Loading efficiency was high for all the formulations and ranged from 93 \pm 2% to 111 \pm 4%. It was significantly lower for the L-PEG-based particles than for the other formulations (ANOVA, $p < 0.05$).

The geometric PSDs are shown in Figure 2, for both blank and sCT-loaded particles. For all the different HP β CD:PEG systems, the PSDs were unimodal. For the blank particles (Figure 2A), a decrease in PEG:HP β CD ratio in the formulation led to a decrease in D_{50} and an increase in the span of the PSD. These changes were concomitant with an increase in the particle specific surface area (Table 1). For most of the formulations, sCT loading did not affect the PSD characteristics (Figure 2B). Figure 2B shows the AD distributions of the 1:1 PEG:HP β CD sCT-loaded particles. With the two types of PEGs, AD distributions were shifted to higher diameter and were broader than the geometric PSD. MMAD and FPF for the L-PEG-based and B-PEG-based particles were 7.3 \pm 0.1 μm , 24.4 \pm 1.3% and 10.4 \pm 0.4 μm , 19.4 \pm 4.4%, respectively.

The formulation process and the change in PEG:HP β CD ratio did not affect the crystallinity of the HP β CD, which was amorphous when analyzed by XRD and DSC. However, the crystallinity of the PEGs in the particles changed depending on the formulation. In the 1:1 PEG:HP β CD formulations, the PEG crystallinity was evident from the presence of the two major Bragg peaks at 19.2 and 23.3 2θ degrees in the diffractograms (data not shown). For this PEG:HP β CD ratio, the addition of sCT did not affect the powder diffractograms. However, a decrease in this ratio to 1:3 led to the XRD amorphization of the PEG in the blank and sCT-loaded particles.

The DSC scans were consistent with the XRD results. Thermograms obtained with the 1:1 PEG:HP β CD systems showed one melting endothermic peak around 60 $^\circ\text{C}$, illustrating the remaining crystallinity of the PEG in these particles. For the 1:3 PEG:HP β CD systems, this endotherm almost disappeared. The average enthalpy of fusion (ΔH_f) recorded for the two types of PEG in the different formulations are reported in Table 1. Using these

Table 2. Particle Surface Free Energy Characteristics^a

PEG/HP β CD ratio	type of PEG	sCT Loaded									
		γ^d (mJ/m ²)		γ^- (mJ/m ²)		γ^+ (mJ/m ²)		γ^{AB} (mJ/m ²)		γ_s^T (mJ/m ²)	
0% RH	40% RH	0% RH	40% RH	0% RH	40% RH	0% RH	40% RH	0% RH	40% RH	0% RH	40% RH
(1/1)	L-PEG	41.5 ± 0.8	37.5 ± 1.1	7.2 ± 0.3	7.1 ± 0.2	0.9 ± 0.0	0.8 ± 0.0	4.9 ± 0.1	4.7 ± 0.1	46.4 ± 0.9	42.3 ± 1.2
	B-PEG	39.4 ± 1.4	36.8 ± 1.1	13.7 ± 0.9	14.6 ± 2.0	1.1 ± 0.1	1.2 ± 0.1	7.8 ± 0.4	8.3 ± 1.0	47.5 ± 1.8	45.0 ± 1.3
Blank Particles											
(1/1)	L-PEG	53.4 ± 2.0		28.8 ± 0.4		2.2 ± 0.1		16 ± 0.4		69.4 ± 1.9	
	B-PEG	40.3 ± 0.9		32.6 ± 0.4		1.8 ± 0.1		15.4 ± 0.5		55.7 ± 1.2	
(1/3)	L-PEG	89.4 ± 1.9		36.1 ± 0.4		3.1 ± 0.1		21.3 ± 0.3		110.7 ± 0.7	
	B-PEG	60.1 ± 1.8		33.6 ± 0.7		4 ± 0.4		23 ± 0.8		83.1 ± 1.0	
100 HP β CD	no	55.7 ± 0.2		7.8 ± 0.5		1.6 ± 0.1		7.1 ± 0.4		62.8 ± 0.6	
Raw Materials											
	0% RH	0% RH		0% RH		0% RH		0% RH		0% RH	
raw L-PEG	37.7 ± 4.0		13.6 ± 1.8		1.1 ± 0.2		7.7 ± 1.0		45.4 ± 5.1		
raw B-PEG	33.4 ± 0.2		17.6 ± 0.2		1.6 ± 0.1		10.6 ± 0.1		44.1 ± 0.1		
raw HP β CD	108.1 ± 17.3		16.9 ± 1.7		2.7 ± 0.4		13.4 ± 1.7		121.6 ± 19.1		

^a Measurements were made at 0% RH for the raw materials and for the blank and sCT-loaded particles. Measurements were also made at 40% RH for the sCT-loaded particles.

values and the ΔH_f of the PEG raw materials (228.5 ± 10.5 J/g and 177.1 ± 2.0 J/g for the L-PEG and B-PEG, respectively), % of crystallinity of the PEG in the particles can be calculated.⁸ $55.4 \pm 3.9\%$ and $65.3 \pm 4.2\%$ of the L-PEG and B-PEG, respectively, was crystalline in the 1:1 PEG:HP β CD blank particles. For the 1:3 PEG:HP β CD blank particles, the crystallinity of the L-PEG was $1.1 \pm 0.2\%$, whereas that of the B-PEG was $6.7 \pm 1.5\%$. The loading of sCT in the 1:1 PEG:HP β CD particles increased the crystallinity of the L-PEG to $66.3 \pm 2.7\%$, whereas it reduced that of the B-PEG to $48.6 \pm 1.8\%$. A similar observation was made for the 1:3 PEG:HP β CD sCT-loaded particles: the % of crystallinity of the L-PEG increased, while it decreased for the B-PEG in comparison to the blank particle.

The mass loss observed by TGA for the sCT-loaded particles upon heating from 25 to 200 °C decreased as the proportion of HP β CD in the formulation decreased (Table 1). The mass loss was around 11, 8, and 2.5 wt %, for the 100% HP β CD, (1:3) PEG:HP β CD, and (1:1) PEG:HP β CD particles, respectively. Similarly, the amount of residual butyl acetate in the particles decreased as the amount of HP β CD decreased.

The γ_s^T , γ_s^d and γ_s^{AB} of the raw materials, blank and sCT-loaded particles measured at 0 and 40% RH are shown in Table 2. The two PEG raw polymers have close γ_s^T values (45.4 ± 5.1 and 44.1 ± 0.1 mJ/m² for L-PEG and B-PEG, respectively), which were lower than for HP β CD ($\gamma_s^T = 121.6 \pm 19.1$ mJ/m²). The higher γ_s^T measured for HP β CD was due to a higher γ_s^d than for the PEGs. However, γ_s^T for the L-PEG-based blank particles was significantly higher than for the B-PEG-based particles, for all PEG:HP β CD ratios investigated. For B-PEG and L-PEG-based blank particles, an increase in HP β CD concentration increased the particles' γ_s^T , due to an increase in both γ_s^d and γ_s^{AB} . For all systems, the major component to γ_s^{AB} was γ^- , which was 2 times higher for the PEG:HP β CD blank particles than for the raw materials. Interestingly, γ_s^T of the blank

HP β CD particles was halved due to a decrease of γ_s^d and γ_s^{AB} in comparison to the unprocessed HP β CD. The loading in sCT in the 1:1 PEG:HP β CD particles reduced γ_s^T with γ_s^d , γ_s^- and γ_s^+ close to that of the PEG raw materials. For these particles, an increase in the RH from 0% to 40% decreased γ_s^T significantly, due to a decrease in γ_s^d . At 40% of RH, γ_s^T observed for the L-PEG-based particles was lower than that observed for the B-PEG-based systems, which was the opposite of what was observed for the blank particles.

Water sorption isotherms and kinetics obtained for the sCT-loaded particles are shown in Figure 3. Kinetics profiles obtained for 1:1 PEG:HP β CD particles presented an increase in mass and then plateaued. The isotherms displayed an adsorption mechanism dominated by type V behavior of the IUPAC classification. From 0 to 70% of RH, the water uptake was similar for the particles made of the two types of PEG. However, after 70% RH, the water uptake for B-PEG-based particles was 3 wt % higher than for L-PEG-based particles. Both 1:1 PEG:HP β CD formulations displayed a closed hysteresis loop in the isotherm. The hysteresis loop obtained with the L-PEG-based particles was small and observed only for high % RH, whereas that obtained with the B-PEG-based particles was observed for the whole isotherm.

A similar hysteresis behavior was detected on the isotherms obtained for the 1:3 PEG:HP β CD formulation. In contrast to the water sorption kinetics observed with the 1:1 PEG:HP β CD particles, kinetics profiles recorded with particles made of 1:3 PEG:HP β CD or just HP β CD were unusual. For most % RH steps, these kinetics displayed a fast increase in mass followed by a slow decrease until the equilibrium condition was reached. This mass loss was reflected in the isotherms as a crossing of the sorption and desorption branches and a loss of mass at the end of the RH cycle. This mass loss increased as the HP β CD concentration was increased in the formulations. After one % RH cycle, 1:3 PEG:HP β CD and HP β CD particles lost 4 and 10 wt %,

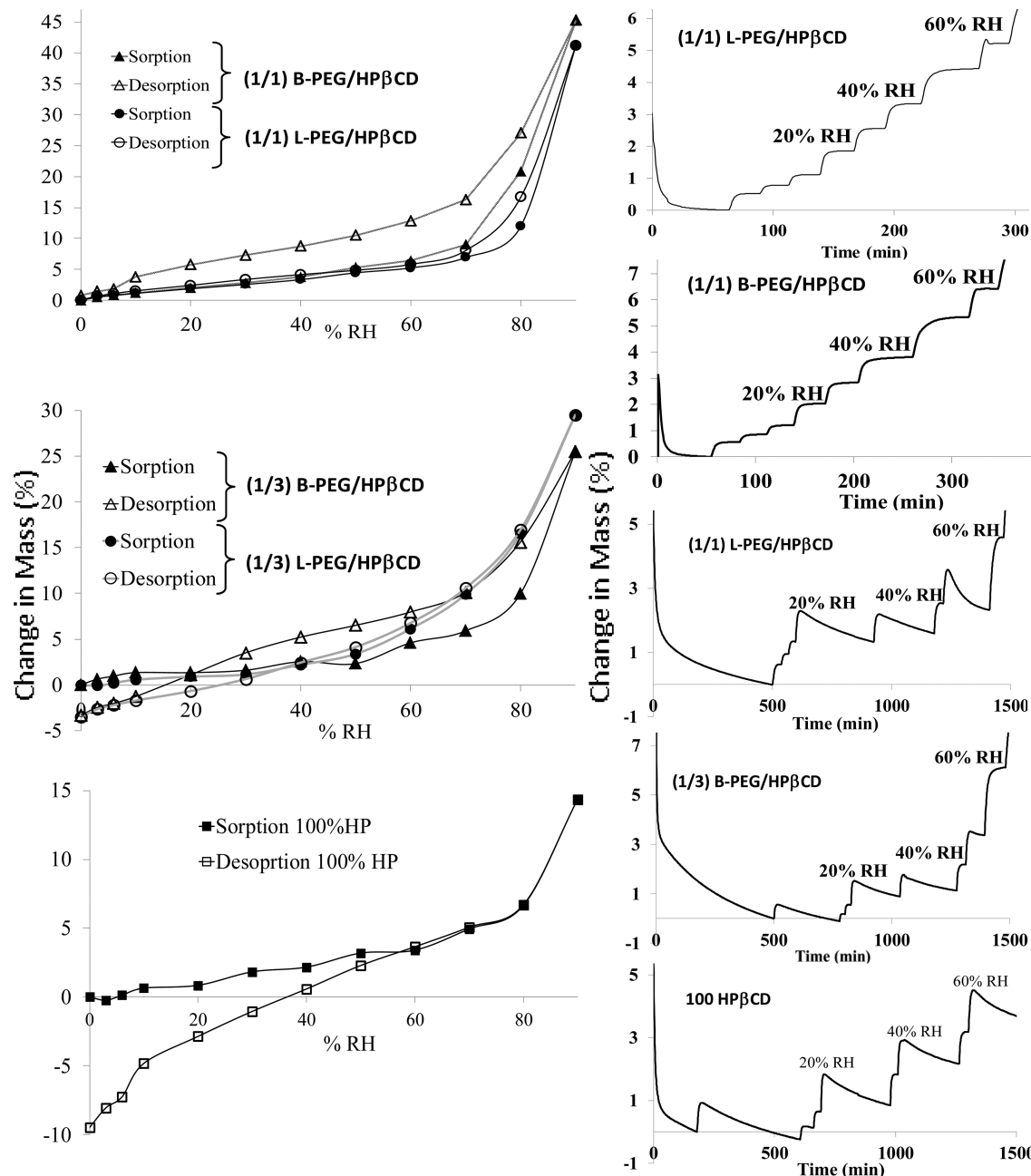


Figure 3. Water sorption—desorption isotherms and water sorption versus time profiles of sCT-loaded particles made of different proportions of PEG and HP β CD.

respectively. These values were close to those obtained by TGA. For all the formulations, the second % RH cycle displayed an adsorption mechanism dominated by type III behavior of the IUPAC classification.

The secondary structure of sCT in the formulations was studied by ATR-FTIR (Figure 4). FTIR has been widely used to study structural changes of protein in solid formulations by monitoring the amide I band in the 1600–1700 cm⁻¹ region.^{21,22} The amide I band of the raw sCT was large and peaked at 1646 cm⁻¹ (Figure 4). The large bandwidth could be due to the amorphous state of the raw sCT. The amide I band acquired from the sCT-loaded particles was narrower and with a maximum shifted to 1658 cm⁻¹ in comparison to the raw sCT. Also, for the

1:3 PEG:HP β CD and HP β CD formulation, new bands located between 1717 and 1735 cm⁻¹ appeared on the sCT spectra. The intensity of these new bands increased with an increase in HP β CD concentration.

Activity of the sCT incorporated in the particles was measured 1, 5, and 6 months after their formulation, by assessing cAMP produced by T47D cells induced by sCT, as previously described.⁸ Activity of sCT was not significantly affected in the PEG-based particles in comparison to a fresh sCT solution. However, in the absence of PEG (i.e., with only HP β CD), the sCT activity was lowered to 63 ± 2%.

sCT A→B P_{app} through Calu-3 cell monolayers, measured using sCT raw material or formulated sCT, are shown in Figure 5A.

P_{app} of sCT alone was $4.97 \pm 0.28 \times 10^{-8}$ cm/s. No significant variation of P_{app} was observed between the sCT raw material and the PEG-based particles. Similarly, no variation of the P_{app} of fluorescein, used as a marker of the tight junction integrity, was observed in the presence of sCT raw material or with the formulations. However, sCT P_{app} measured after its formulation with only HP β CD was significantly higher than for the sCT alone. In this latter experiment, the apical HP β CD concentration was 0.4 wt %. Thus, we measured the sCT P_{app} in the presence of different HP β CD concentrations (from 0.4 to 6.4 wt %) to evaluate the effect of HP β CD on sCT P_{app} (Figure 5B). In these experiments, no significant change in sCT P_{app} was observed. However, in the presence of 1.6 wt % of PEGs added to 1.6 wt % of HP β CD a significant 2-fold reduction in sCT P_{app} was measured.

Various mechanisms could explain the reduction in sCT P_{app} observed. One of these could be the increase in buffer viscosity caused by the excipients. Hence, μ (mPa·s) of buffers containing different concentrations of PEG alone or PEG and HP β CD was evaluated (Figure 6). The viscosity of the buffers increased with

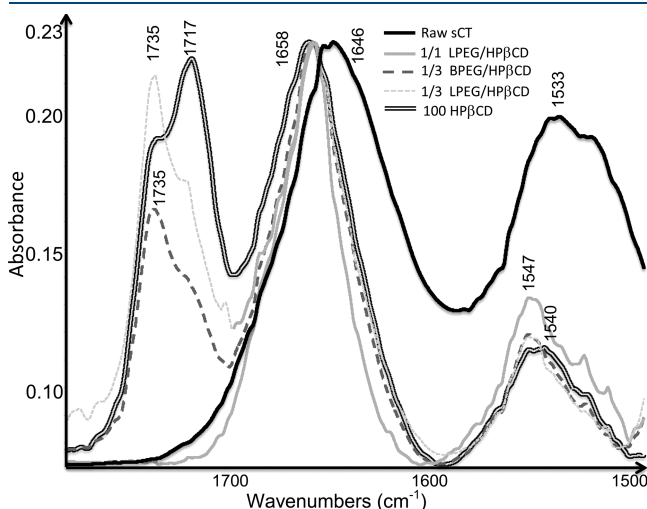


Figure 4. ATR-FTIR spectra of L-PEG and B-PEG sCT-loaded dry particles. As the 1:1 PEG:HP β CD spectra were overlapping, only L-PEG:HP β CD was shown.

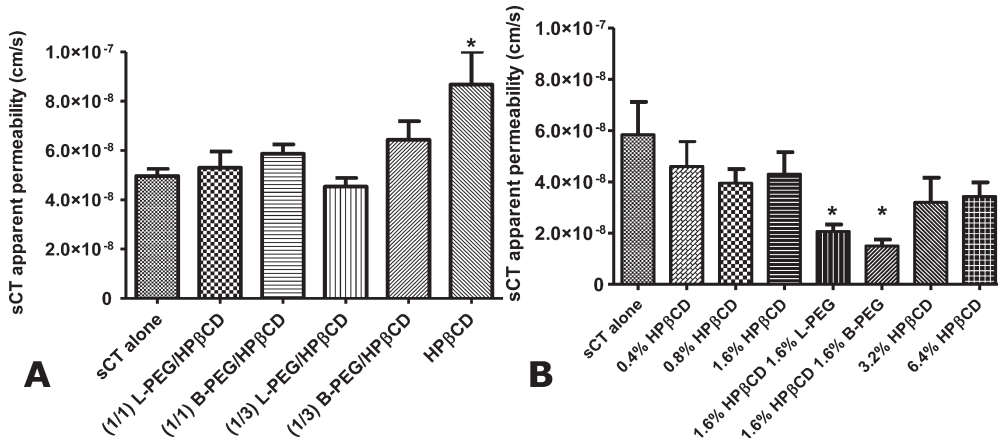


Figure 5. Apical-to-basolateral apparent permeability of sCT across Calu-3 cell monolayers. (A) Measurements were made in the presence of unprocessed or formulated sCT. (B) Measurements were made in the presence of unprocessed sCT and different concentrations of HP β CD and PEGs. Apical sCT concentration was $200 \mu\text{g/mL}$ in all cases. Results are mean values after 60 min \pm SEM ($n = 3$; * $P < 0.05$).

PEG concentration and was 10-times higher than water for 20 wt % PEG. For the PEG concentration range studied, buffer solutions containing L-PEG had a higher μ than for B-PEG. The addition of HP β CD to the PEG, at the same concentration, increased the μ of the buffer. The viscosity of a buffer made of 20 wt % of L-PEG and 20 wt % of HP β CD was 2 times higher than a solution made of L-PEG only.

Based on the biopharmaceutical properties obtained for the sCT formulations, *in vivo* evaluation was done using the 1:1 PEG:HP β CD particles. Each sCT plasma concentration versus time profile obtained after sCT administration was fitted using a two-compartment model. Averaged curves are displayed in Figure 7, and the values of the relevant pharmacokinetic parameters are listed in the Table 3.

After sCT iv bolus administration, the log plot of the plasma concentration versus time profiles showed two phases: a first short phase, characterized by a $t_{1/2-\alpha}$ of 2.6 ± 0.1 min that corresponds to the distribution of the sCT in the peripheral compartment, and a second phase, controlled by the sCT elimination process, observed after 10 min and characterized by a $t_{1/2-\beta}$ of 34.7 ± 4.4 min.

The sCT plasma concentration versus time profiles after pulmonary administration of sCT solution at $100 \mu\text{g/kg}$ (Figure 7B) showed a very short absorption phase ($K_a = 0.456 \pm 0.158 \text{ min}^{-1}$). F measured for this dose was $11.3 \pm 1.7\%$. Interestingly, the pulmonary administration of sCT-loaded

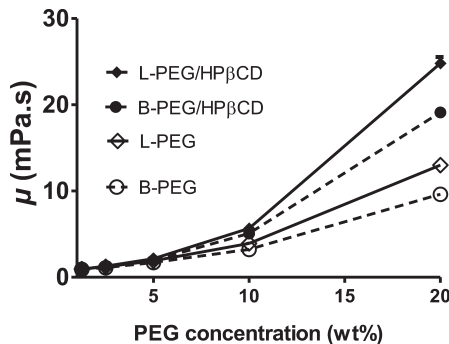
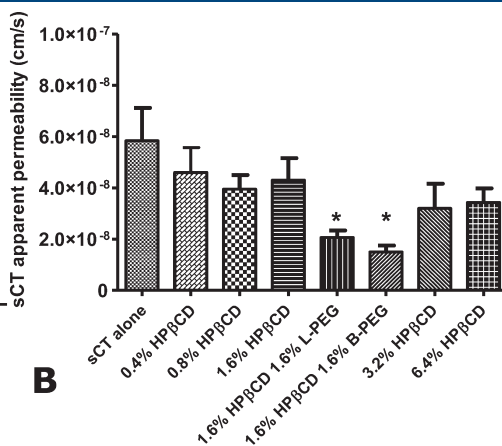


Figure 6. Viscosity of L-PEG and B-PEG solutions. Viscosity was measured for pure PEG solution and for PEG:HP β CD solution containing the same concentration of both materials. $T = 37^\circ\text{C}$.



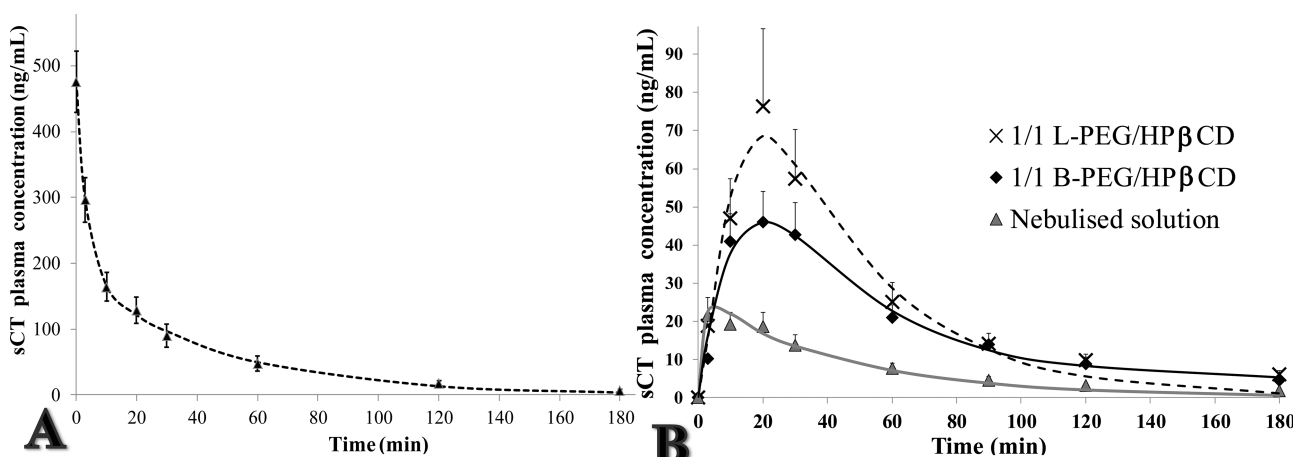


Figure 7. sCT plasma concentration versus time profiles after (A) intravenous administration of sCT solution at a dose of 100 $\mu\text{g}/\text{kg}$ and (B) pulmonary aerosolization of sCT solution, (1:1) L-PEG:HP β CD-based particles, and (1:1) B-PEG:HP β CD-based particles at a dose of 100 $\mu\text{g}/\text{kg}$. Curves represent mean \pm SEM ($n = 6-7$).

Table 3. Pharmacokinetic Parameters after Two-Compartment Analysis of the sCT Plasma Concentration versus Time Profiles^a

	iv	nebulized solution	L-PEG	B-PEG
AUC $_{\infty}$ (min · ng/mL/ $\mu\text{g} \cdot \text{kg}$)	124.8 \pm 13.1	14.1 \pm 2.1	31.1 \pm 6.7*	21.2 \pm 2.2
T _{max} (min)		4.2 \pm 1.1	20 \pm 0.0	18.3 \pm 2.9
C _{max} (ng/mL)	467 \pm 35	24.1 \pm 4.5	68.2 \pm 15.1	48.1 \pm 7.5
K _{el} (min ⁻¹)	0.053 \pm 0.007	0.037 \pm 0.003	0.041 \pm 0.002	0.045 \pm 0.003
CL (mL/min/kg)	9.1 \pm 1.0	8.8 \pm 0.2	8.6 \pm 0.1	8.7 \pm 0.2
K _a (min ⁻¹)		0.456 \pm 0.060	0.167 \pm 0.006*	0.168 \pm 0.012*
F (%)	100 \pm 10.7	11.3 \pm 1.7	26.3 \pm 5.5*	17.0 \pm 1.7

^a Mean \pm SEM ($n = 6-7$); *P < 0.05, indicating a significant difference between the mean values of the PK parameters obtained after sCT pulmonary administration.

particles significantly prolonged the absorption phase. The absorption rate constants calculated for the L-PEG-based and B-PEG-based formulations were $0.167 \pm 0.005 \text{ min}^{-1}$ and $0.168 \pm 0.012 \text{ min}^{-1}$, respectively. Moreover, F after lung insufflation of the 1:1 L-PEG:HP β CD particles was significantly higher ($26.3 \pm 5.5\%$) than after nebulization of sCT solution.

4. DISCUSSION

Existing aerosol systems are still poorly designed for the systemic administration of peptides via the lung. Peptides in solution are often unstable, and powders formulated with sugars are often sensitive to the RH % and are too cohesive.⁴ Thus, the use of PEG, an excipient with low γ_S^T , may result in stabilization of the peptide and the formulation of a powder with low cohesiveness. We have previously reported on the use of a butyl acetate/methanol solvent mixture to produce sugar-based nanoporous microparticles by spray drying.²³ These microparticles have advantageous properties for pulmonary peptide delivery. Also, we used the same solvent combination in this study with the aim of producing porous microparticles of PEG and HP β CD. However, as shown by experimental results, a high concentration in HP β CD in the formulation led to an increase in the amount of residual butyl acetate in the particles. For example, the appearance of bands between 1717 and 1735 cm⁻¹ on the sCT spectra acquired from the 1:3 PEG:HP β CD and HP β CD particles

(Figure 4) can be attributed to C=O vibration of the butyl acetate. Also, particles made of 1:3 PEG:HP β CD or HP β CD displayed a mass loss at the end of the water sorption isotherm, also observed on each water sorption stage (Figure 3). These mass losses were close to those observed by TGA upon heating and could be attributed to the evaporation of the butyl acetate, initially bonded to the HP β CD. This capacity to retain the butyl acetate is most likely related to the ability of β CD to complex the butyl acetate, and decrease its volatility.^{24,25} Nevertheless, butyl acetate belongs to the less toxic class (3) in the organic solvent classification.²⁶ The absorption of such solvent is limited to not more than 50 mg per day (corresponding to 5000 ppm of solvent, assuming a formulation mass of 10 g administered daily). For the 1:1 PEG:HP β CD formulations the amount of butyl acetate was much lower than this authorized limit value. Thus this residual butyl acetate should not limit the use of these formulations.

The morphology of the PEG:HP β CD blank particles was influenced by the type of PEG used and by the PEG:HP β CD ratio (Figure 1). At a 1:1 PEG:HP β CD ratio, the B-PEG facilitated the formation of nanoparticles attached to microparticles in comparison to the L-PEG. A decrease in the PEG:HP β CD ratio suppressed the difference between the PEGs in terms of particle morphology and enhanced the formation of attached nanoparticles. Spray drying of HP β CD alone strongly reduced the adhesion of the nanoparticles onto the microparticles. Thus, these PEGs having a low T_g and T_m ²⁷ allow the nanoparticles to

agglomerate on the microparticles, producing narrower PSD. However, a minimal amount of HP β CD is needed, as PEG alone spray dried from standard solvents produces large aggregates.^{8,10}

The increase in the number of nanoparticles shifted the geometric PSD (Figure 2A), and led to an increase in the specific surface area (Table 1). A linear relationship between the specific surface areas versus $1/D_{50}$ can be plotted with a good r^2 (0.91), indicating a low porosity of the particles. The increase in the particle surface roughness provided by the nanoparticle layer created by a decrease in the PEG:HP β CD ratio should improve the particle aerosolization.²⁸ However, a decrease in this ratio also led to a strong increase in γ_s^T (Table 2), which should increase the particles' agglomeration ability, and adversely impact on the particle aerodynamic behavior. This increase in γ_s^T could be attributed to the increase in the proportion of HP β CD molecules at the particle surface, as HP β CD raw material has a higher γ_s^T than PEGs. However, blank HP β CD particles had a lower γ_s^T than the HP β CD raw material, suggesting a relaxation of the amorphous HP β CD at the particle surface after processing. Also, the % of PEG crystallinity in the blank particles decreased as the ratio of HP β CD was increased (Table 1). Therefore, the increase in amorphous PEG present at the particle surface could likewise result in an increase in γ_s^T . The γ_s^T for the L-PEG-based blank particles was significantly higher than for the B-PEG-based particles and the % of crystallinity of the L-PEG in the blank particles was lower than for the B-PEG ones (Table 1). Thus, different amount of amorphous PEG located at the particle surface is likely to have resulted in high particle γ_s^T .

The amount of amorphous PEG seemed to be controllable by the PEG:HP β CD ratio. L-PEG appeared to interact more with HP β CD as its % of crystallinity was decreased to a larger extent than B-PEG in the blank particles. In fact, two types of interaction can occur between PEG and HP β CD. First, HP β CD can be threaded onto the PEG chain via its cavity, resulting in a poly-pseudorotaxane-like assembly.²⁹ However, as the β CD cavity is too large to "complex" the PEG, this assembly should be transitory in solution. Second, HP β CD can develop hydrogen bond with the ether group of the PEGs, through its hydroxyl functions. The difference in interactions between HP β CD and either L-PEG or B-PEG should be related to the different spatial conformation between the two types of PEG.

The addition of 5 wt % of sCT in particles changed their morphologies, and decreased the amount and size of nanoparticles, making the PSD more homogeneous. Similarly, sCT changed the % of PEG crystallinity and reduced particle γ_s^T . For the L-PEG-based particles, sCT increased the % of PEG crystallinity, while the % crystallinity decreased for the B-PEG-based particles. These different behaviors could be due to the competitive interactions involved between the PEG, HP β CD and sCT. The increase in L-PEG % of crystallinity could be the result of strong interactions between HP β CD and sCT, as was observed by Fridbjörg Sigurjónsdóttir et al.,¹¹ decreasing the possibility of interactions between the L-PEG and HP β CD. However, the decrease in B-PEG % of crystallinity could be due to the development of more interactions with the sCT alone or with sCT-HP β CD complex than those developed in the blank particles alone. In fact, PEG is known to stabilize drug/cyclodextrin complexes through the formation of ternary complexes.³⁰

Also, the decrease in γ_s^T measured for the 1:1 L-PEG:HP β CD sCT-loaded particles could be the result of more crystalline PEG polymer present at the particle surface, enhanced by the presence of sCT. Actually, the surface free energy profile of

these particles was comparable to that of PEG raw material. The better aerosolization properties of L-PEG-based particles compared to B-PEG-based particles could be explained by the lower γ_s^T measured for the L-PEG-based particles than for B-PEG-based ones. However, for these particles, the AD distributions were shifted to higher values in comparison to the geometric PSD, suggesting some particle aggregation. Nevertheless, γ_s^T of these particles (Table 2) were lower than values measured for aerosols that are routinely inhaled, such as salbutamol (65 mJ/m^2) or budenoside (53.7 mJ/m^2).³¹

Because the amount of free water in a powder influences its physical stability and respirability, water–particle interaction was evaluated by DVS for the sCT-loaded particles (Figure 3). For 1:1 PEG:HP β CD particles, the water uptake isotherm profiles showed a low water uptake up to 70% of RH, suggesting good physical stability. Additionally, for these particles, an increase in the RH from 0 to 40% decreased γ_s^T significantly, which should be beneficial for particle aerosolization. Studies have shown that water molecules bound to PEG are structurally distinct from bulk water and partly responsible for the low protein adsorption on surfaces grafted with PEG.³² This particular organization of water molecules could explain the decrease in γ_s^T observed after an increase in RH %. Water sorption isotherms also showed that 1:1 B-PEG:HP β CD particles are able to retain more water than the 1:1 L-PEG:HP β CD particles, resulting in a hysteresis loop in the isotherm for the B-PEG-based particles. This ability to retain water could create capillary forces between the particles and explain the lower aerosolization properties of the 1:1 B-PEG:HP β CD particles compared to the 1:1 L-PEG:HP β CD particles.

Salmon calcitonin conformation study performed by FTIR showed a narrowing and a shift to higher wavenumbers of the sCT amide I band in FTIR spectra acquired from the particles compared to the spectra recorded for the sCT raw material (Figure 4). This shows a higher degree of organization of the sCT in the particles and could be assigned to an increase in α -helix-like structure of sCT.^{21,22} Additionally, no signal of sCT aggregation was observed in any of the spectra, which would be expected around $1625 - 1630 \text{ cm}^{-1}$.³³ The bioactivity of sCT in the particles was calculated using the sCT loading, and thus it reflected the activity of the intact sCT present in the particles. sCT bioactivity was not significantly affected in the PEG-based particles. Similar results were observed with PEG:PVP-based sCT-loaded particles prepared by spray drying.⁸ In the absence of PEG, the sCT activity was lowered to $63 \pm 2\%$, suggesting that the PEG polymers allowed the integrity of the sCT to be maintained. However, it has been shown that various β -cyclodextrin (β CD) derivatives can function as aggregation suppressors for a wide range of proteins¹⁶ and with sCT.¹¹ This effect is often ascribed to their affinity for aromatic amino acids, whose surface exposure would otherwise lead to protein association. Also, sCT could form a complex with HP β CD through the aromatic His-17. Therefore, the lower sCT activity observed in the particles composed only of HP β CD as the excipient could be due to the high degree of interaction between sCT and HP β CD, inhibiting or hindering the interaction of sCT with its membrane receptor. This decrease in affinity of sCT-HP β CD complex relative to the free sCT could happen if amino acid residues involved in receptor binding are "masked" by the cyclodextrin.

The apparent permeability of a molecule describes how fast it passes through endothelial and epithelial cells. It is one of the parameters which determine the extent and fraction of absorption. The A→B P_{app} of sCT alone across Calu-3 monolayer, a

commonly used model representing the respiratory mucosa,³⁴ was very low ($4.97 \pm 0.28 \times 10^{-8}$ cm/s), which was consistent with values measured on Caco-2 cell monolayer ($1.71 \pm 0.32 \times 10^{-7}$ cm/s).³⁵ This low P_{app} value suggests low sCT lung absorption. The P_{app} of sCT (peptide of 3.4 kDa) was close to that obtained for a FITC-labeled dextran of 4.4 kDa ($1.71 \pm 0.25 \times 10^{-8}$ cm/s) across human alveolar cell monolayer, having a similar TEER.³⁶ Also, sCT is known to easily aggregate,¹¹ but this P_{app} value suggests that intact monomeric form of sCT was transported across the Calu-3 monolayer by passive size-dependent diffusion only. Due to the size and polarity of sCT, its transport should be via the paracellular route.

The absence of a significant change in P_{app} of sCT and fluorescein in the presence of PEG-based formulated sCT (Figure 5A) shows the innocuity of the excipients towards the Calu-3 cells at the concentration used. The sCT P_{app} measured after its formulation with HP β CD as a single excipient was significantly higher than the P_{app} measured for the sCT alone. However, no significant increase in sCT P_{app} with an increase in HP β CD concentration in the buffer was observed (Figure 5B). A higher degree of interaction between sCT and HP β CD after formulation than after simple contact in buffer could explain the difference of P_{app} observed between formulated and unprocessed sCT. In fact, as shown by Fridbjörg Sigurjónsdóttir et al.,¹¹ HP β CD can protect sCT against peptidase action, such as trypsin and α -chymotrypsin. These enzymes are present in Calu-3 cells as well as in human respiratory epithelial barrier *in situ* and are a limiting factor for pulmonary peptide absorption.^{4,37,38} Therefore, the higher sCT P_{app} measured in the presence of the HP β CD formulation could be the result of a better protection against these enzymes. In the presence of 1.6 wt % of L-PEG added to 1.6 wt % of HP β CD, a significant 2.4-fold reduction in sCT P_{app} was measured. The decrease in sCT P_{app} with the increase in excipients concentration could be related to the increase in the viscosity between the Calu-3 paracellular aqueous channels, caused by these excipients. In fact, 1.6 wt % of L-PEG + HP β CD increased the buffer's viscosity 1.59-fold.

The PK study of sCT was well described with a two-compartmental model after iv bolus injection. Similar analyses were previously done after iv infusion³⁹ administrations, but at lower doses. Most of the PK parameters, such as $t_{1/2}$ or CL,^{7,39,40} were similar between the studies and our data. These values showed that the sCT quickly disappears from plasma and that high frequency blood sampling should be performed to fully understand the PK. From the PK parameters obtained after iv injection, we further modeled the pulmonary absorption of sCT from the insufflated formulations or solution, assuming a first order absorption mechanism with immediate release of the sCT from the particles. The estimation of the K_a after releasing sCT from the lung allowed comparison between the sCT formulations and solution. The sCT plasma concentration versus time profiles after pulmonary administration of sCT solution at 100 μ g/kg (Figure 7B) showed a very short absorption phase, characterized by a high absorption rate constant ($0.456 \pm 0.158 \text{ min}^{-1}$) and a T_{max} lower than 3 min. These results showed a faster absorption than previously published, mainly because the blood sampling performed in the other studies started only at 10 or 15 min after administration.

sCT bioavailability measured for this dose was 11.4%, which was similar to F values reported by studies which ranged from 11.5 to 18%,^{1,41,42} and the AUC value obtained by Youn et al.⁷ (10.7 $\text{min} \cdot \text{ng/mL}/\mu\text{g} \cdot \text{kg}$) was close to that calculated in our

study (Table 3). These low F values are in agreement with the low sCT P_{app} values measured across the Calu-3 monolayer. The decrease in K_a in the presence of particles in comparison to the solution was statistically significant and indicates that formulations can extend the T_{max} . The increase in T_{max} was comparable to those achieved by chemically binding PEG 2 kDa to sCT.⁷ Moreover, the sCT F value observed after lung insufflation of the 1:1 L-PEG:HP β CD particles was significantly higher (2.3-fold) than after nebulization of sCT solution. In comparison, chemical binding of PEG to sCT led to a higher AUC (2.4- to 7.3-fold, depending on the PEG M_w).⁷

The relative bioavailability of sCT measured after nasal administration of a spray of Fortical ranged from 0.3 to 30%, with a mean of 3% of the F value obtained after sCT intramuscular injection.² The pulmonary delivery of peptides as a route for systemic drug delivery is intended to improve systemic bioavailability and reduce the pharmacokinetic variability. Compared to the relative F value obtained using Fortical, the absolute sCT F obtained after nebulization of the 1:1 L-PEG:HP β CD particles was higher and less variable ($26.3 \pm 5.5\%$).

When particles land on the fine layer of the lung epithelial fluid, sCT and excipient concentration can be high immediately after the particle dissolution. High PEG and HP β CD concentration could lead to a high local viscosity, as suggested by μ measurements, and may be responsible for the increase in T_{max} and AUC. This high viscosity could decrease sCT P_{app} but also slow down clearance and/or degradation mechanisms involved in sCT elimination. Furthermore, the possible interaction/complexation of sCT with HP β CD should reduce the lung peptidase action as observed by Kobayashi et al.,¹³ and also contribute to the increase in sCT bioavailability.

5. CONCLUSIONS

This study offered a new approach to the formulation of active peptide loaded microparticles suitable for pulmonary administration. It shows that PEG-based microparticles with different physicochemical properties resulted in modified sCT pharmacokinetic profiles and allowed the bioavailability of sCT following pulmonary administration to be significantly ($p < 0.05$) enhanced.

■ AUTHOR INFORMATION

Corresponding Author

*School of Pharmacy and Pharmaceutical Sciences, University of Dublin, Trinity College, Dublin 2, Ireland. Tel: +353-1-896-1444. Fax: +353-1-896-2783. E-mail: healyam@tcd.ie.

■ ACKNOWLEDGMENT

This study was funded by the Irish Drug Delivery Research Network, a Strategic Research Cluster grant (07/SRC/B1154) under the National Development Plan cofunded by EU Structural Funds and Science Foundation Ireland.

■ REFERENCES

- (1) Patton, J. S. Pulmonary delivery of drugs for bone disorders. *Adv. Drug Delivery Rev.* **2000**, *42* (3), 239–248.
- (2) Walsh, G. Biopharmaceutical benchmarks 2006. *Nat. Biotechnol.* **2006**, *24* (7), 769–776.
- (3) Stevenson, C. L. Advances in peptide pharmaceuticals. *Curr. Pharm. Biotechnol.* **2009**, *10* (1), 122–137.

- (4) Patton, J. Breathing life into protein drugs. *Nat. Biotechnol.* **1998**, *16* (2), 141–143.
- (5) Bailon, P.; Berthold, W. Polyethylene glycol-conjugated pharmaceutical proteins. *Pharm. Sci. Technol. Today* **1998**, *1* (8), 352–356.
- (6) Frokjaer, S.; Otzen, D. E. Protein drug stability: A formulation challenge. *Nat. Rev. Drug Discovery* **2005**, *4* (4), 298–306.
- (7) Youn, Y. S.; Kwon, M. J.; Na, D. H.; Chae, S. Y.; Lee, S.; Lee, K. C. Improved intrapulmonary delivery of site-specific PEGylated salmon calcitonin: Optimization by PEG size selection. *J. Controlled Release* **2008**, *125* (1), 68–75.
- (8) Tewes, F.; Tajber, L.; Corrigan, O. I.; Ehrhardt, C.; Healy, A. M. Development and characterisation of soluble polymeric particles for pulmonary peptide delivery. *Eur. J. Pharm. Sci.* **2010**, *41* (2), 337–352.
- (9) Wattendorf, U.; Merkle, H. P. PEGylation as a tool for the biomedical engineering of surface modified microparticles. *J. Pharm. Sci.* **2008**, *97* (11), 4655–4669.
- (10) Corrigan, D. O.; Healy, A. M.; Corrigan, O. I. The effect of spray drying solutions of polyethylene glycol (PEG) and lactose/PEG on their physicochemical properties. *Int. J. Pharm.* **2002**, *235* (1–2), 193–205.
- (11) Fridbjörg Sigurjónsdóttir, J.; Loftsson, T.; Másson, M. Influence of cyclodextrins on the stability of the peptide salmon calcitonin in aqueous solution. *Int. J. Pharm.* **1999**, *186* (2), 205–213.
- (12) Nakate, T.; Yoshida, H.; Ohike, A.; Tokunaga, Y.; Ibuki, R.; Kawashima, Y. Improvement of pulmonary absorption of cyclopeptide FK224 in rats by co-formulating with beta-cyclodextrin. *Eur. J. Pharm. Biopharm.* **2003**, *55* (2), 147–154.
- (13) Kobayashi, S.; Kondo, S.; Juni, K. Pulmonary delivery of salmon calcitonin dry powders containing absorption enhancers in rats. *Pharm. Res.* **1996**, *13* (1), 80–83.
- (14) Salem, L. B.; Bosquillon, C.; Dailey, L. A.; Delattre, L.; Martin, G. P.; Evrard, B.; Forbes, B. Sparing methylation of β -cyclodextrin mitigates cytotoxicity and permeability induction in respiratory epithelial cell layers in vitro. *J. Controlled Release* **2009**, *136* (2), 110–116.
- (15) Tewes, F.; Brillault, J.; Couet, W.; Olivier, J. C. Formulation of rifampicin-cyclodextrin complexes for lung nebulization. *J. Controlled Release* **2008**, *129* (2), 93–99.
- (16) Brewster, M. E.; Loftsson, T. Cyclodextrins as pharmaceutical solubilizers. *Adv. Drug Delivery Rev.* **2007**, *59* (7), 645–666.
- (17) Schultz, J.; Lavielle, L.; Martin, C. The role of the interface in carbon-fiber epoxy composites. *J. Adhes.* **1987**, *23* (1), 45–60.
- (18) Van Oss, C. J.; Good, R. J.; Chaudhury, M. K. Additive and nonadditive surface tension components and the interpretation of contact angles. *Langmuir* **1988**, *4* (4), 884–891.
- (19) Della Volpe, C.; Siboni, S. Some reflections on acid-base solid surface free energy theories. *J. Colloid Interface Sci.* **1997**, *195* (1), 121–136.
- (20) Higuti, I. H.; Da Silva, P. A.; Papp, J.; De Eiróz Okiyama, V. M.; De Andrade, E. A.; De Abreu Marcondes, A.; Do Nascimento, A. J. Colorimetric determination of α and β -cyclodextrins and studies on optimization of CGTase production from *B. Firmus* using factorial designs. *Braz. Arch. Biol. Technol.* **2004**, *47* (6), 837–841.
- (21) Chan, H. K.; Clark, A. R.; Feeley, J. C.; Kuo, M. C.; Lehrman, S. R.; Pikal-Cleland, K.; Miller, D. P.; Vehring, R.; Lechuga-Ballesteros, D. Physical Stability of Salmon Calcitonin Spray-Dried Powders for Inhalation. *J. Pharm. Sci.* **2004**, *93* (3), 792–804.
- (22) Yang, M.; Velaga, S.; Yamamoto, H.; Takeuchi, H.; Kawashima, Y.; Hovgaard, L.; van de Weert, M.; Frokjaer, S. Characterisation of salmon calcitonin in spray-dried powder for inhalation. Effect of chitosan. *Int. J. Pharm.* **2007**, *331* (2), 176–181.
- (23) Ní Ógáin, O.; Li, J.; Tajber, L.; Corrigan, O. I.; Healy, A. M. Particle engineering of materials for oral inhalation by dry powder inhalers. i - Particles of sugar excipients (trehalose and raffinose) for protein delivery. *Int. J. Pharm.* **2011**, *405* (1–2), 23–35.
- (24) Tobitsuka, K.; Miura, M.; Kobayashi, S. Interaction of cyclodextrins with aliphatic acetate esters and aroma components of La France pear. *J. Agric. Food Chem.* **2005**, *53* (13), 5402–5406.
- (25) Jones, S. P.; Parr, G. D. Polarographic detection of beta-cyclodextrin inclusion complexes. *Int. J. Pharm.* **1986**, *33* (1–3), 105–114.
- (26) *Impurities: Guideline for Residual Solvents*; ICH Topic Q3C (R5): March 2011; pp 1–26.
- (27) Verheyen, S.; Augustijns, P.; Kinget, R.; Van Den Mooter, G. Melting behavior of pure polyethylene glycol 6000 and polyethylene glycol 6000 in solid dispersions containing diazepam or temazepam: A DSC study. *Thermochim. Acta* **2001**, *380* (2), 153–164.
- (28) Edwards, D. A.; Hanes, J.; Caponetti, G.; Hrkach, J.; Ben-Jebria, A.; Eskew, M. L.; Mintzes, J.; Deaver, D.; Lotan, N.; Langer, R. Large porous particles for pulmonary drug delivery. *Science* **1997**, *276* (5320), 1868–1871.
- (29) Loethen, S.; Kim, J.-M.; Thompson, D. H. Biomedical Applications of Cyclodextrin Based Polyrotaxanes. *Polym. Rev.* **2007**, *47* (3), 383–418.
- (30) Moya-Ortega, M.; Messner, M.; Jansook, P.; Nielsen, T.; Wintgens, V.; Larsen, K.; Amiel, C.; Sigurdsson, H.; Loftsson, T. Drug loading in cyclodextrin polymers: dexamethasone model drug. *J. Inclusion Phenom. Macroyclic Chem.* **2011**, *69* (3), 377–382.
- (31) Traini, D.; Rogueda, P.; Young, P.; Price, R. Surface Energy and Interparticle Force Correlation in Model pMDI Formulations. *Pharm. Res.* **2005**, *22* (5), 816–825.
- (32) Kim, J.; Qian, W.; Al-Saigh, Z. Y. Measurements of water sorption enthalpy on polymer surfaces and its effect on protein adsorption. *Surf. Sci.* **2011**, *605* (3–4), 419–423.
- (33) Bauer, H. H.; Muller, M.; Goette, J.; Merkle, H. P.; Fringeli, U. P. Interfacial adsorption and aggregation associated changes in secondary structure of human calcitonin monitored by ATR-FTIR spectroscopy. *Biochemistry* **1994**, *33* (40), 12276–12282.
- (34) Sporty, J. L.; Horálková, L.; Ehrhardt, C. In vitro cell culture models for the assessment of pulmonary drug disposition. *Expert Opin. Drug Metab. Toxicol.* **2008**, *4* (4), 333–345.
- (35) Song, K. H.; Chung, S. J.; Shim, C. K. Enhanced intestinal absorption of salmon calcitonin (sCT) from proliposomes containing bile salts. *J. Controlled Release* **2005**, *106* (3), 298–308.
- (36) Elbert, K. J.; Schäfer, U. F.; Schäfers, H.-J.; Kim, K.-J.; Lee, V. H. L.; Lehr, C.-M. Monolayers of Human Alveolar Epithelial Cells in Primary Culture for Pulmonary Absorption and Transport Studies. *Pharm. Res.* **1999**, *16* (5), 601–608.
- (37) Baginski, L.; Tachon, G.; Falson, F.; Patton, J. S.; Bakowsky, U.; Ehrhardt, C. Reverse Transcription Polymerase Chain Reaction (RT-PCR) analysis of proteolytic enzymes in cultures of human respiratory epithelial cells. *J. Aerosol Med. Pulm. Drug Delivery* **2011**, *24* (2), 89–101.
- (38) Baginski, L.; Tewes, F.; Buckley, S. T.; Healy, A. M.; Bakowsky, U.; Ehrhardt, C. Investigations into the Fate of Inhaled Salmon Calcitonin at the Respiratory Epithelial Barrier. *Pharm. Res.* **2011**, *1*–10.
- (39) Miyazaki, M.; Nakade, S.; Iwanaga, K.; Morimoto, K.; Kakemi, M. Estimation of Bioavailability of Salmon Calcitonin from the Hypocalcemic Effect in Rats (I): Pharmacokinetic-Pharmacodynamic Modeling Based on the Endogenous Ca Regulatory System. *Drug Metab. Pharmacokinet.* **2003**, *18* (6), 350–357.
- (40) Song, K. H.; An, H. M.; Kim, H. J.; Ahn, S. H.; Chung, S. J.; Shim, C. K. Simple liquid chromatography-electrospray ionization mass spectrometry method for the routine determination of salmon calcitonin in serum. *J. Chromatogr. B: Anal. Technol. Biomed. Life Sci.* **2002**, *775* (2), 247–255.
- (41) Komada, F.; Iwakawa, S.; Yamamoto, N.; Sakakibara, H.; Okumura, K. Intratracheal delivery of peptide and protein agents: absorption from solution and dry powder by rat lung. *J. Pharm. Sci.* **1994**, *83* (6), 863–867.
- (42) Kobayashi, S.; Kondo, S.; Juni, K. Critical factors on pulmonary absorption of peptides and proteins (diffusional barrier and metabolic barrier). *Eur. J. Pharm. Biopharm.* **1996**, *4* (6), 367–372.